Solar Energy Materials & Solar Cells 141 (2015) 225–231

Contents lists available at ScienceDirect

Solar Energy Materials & Solar Cells

journal homepage: www.elsevier.com/locate/solmat

Ultra-thin, high performance crystalline silicon tandem cells fabricated on a glass substrate

Guijun Li*, He Li, Jacob Ho, Man Wong, Hoi-Sing Kwok

State Key Lab on Advanced Displays and Optoelectronics Technologies, Department of Electronic and Computer Engineering, Hong Kong University of Science and Technology, Clear Water Bay, Kowloon, Hong Kong

ARTICLE INFO

Article history:
Received 19 January 2015
Received in revised form
26 May 2015
Accepted 28 May 2015
Available online 17 June 2015

Keywords:
Ultrathin c-Si
Solar cell
Anodic bonding
Conformal deposition
Inverted nanopyramid
Light trapping

ABSTRACT

Ultrathin silicon provides a viable pathway towards the realization of photovoltaic devices aimed at reducing material usage, utilizing low quality material and diversifying their application. However, solar cells based on the ultrathin film reported thus far are still far from fully optimized compared with their crystalline, wafer-based counterparts due to insufficient light absorption. Furthermore, fabrication of these ultrathin devices on an inexpensive substrate, such as glass and plastic, is still a critical issue at present. Here we present an approach to fabricate ultrathin, high performance silicon solar cells with a tandem structure on a glass substrate. The strategy involves transferring the ultrathin film to the glass substrate by applying an anodic bonding process, introducing a nanoscale inverted pyramid light trapping structure that is suitable for conformal deposition to enhance light absorption, and engineering doped layers to avoid parasitic optical and electrical losses. We demonstrate a-Si/c-Si tandem solar cells with high efficiencies of up to 13.6%, using a 300 nm thick a-Si top cell and a sub-8 μm-thick silicon bottom cell. This significant improvement of the efficiency is achieved even without the complicated passivation process normally applied in high-efficiency silicon solar cells. Our results are an important step toward high-efficiency ultrathin solar cells for the future.

1. Introduction

Crystalline silicon solar cells with thicknesses of 180–300 μm have dominated the photovoltaic industry with a market share around 80–90%, for decades. The cost of the silicon material used still accounts for around 35% of the total module cost; [1] thus reducing the thickness of the silicon from 180–300 μm to sub -10 μm, will definitely have a significant impact on driving the cost reduction of photovoltaic electricity substantially. An ultra-thin absorbing layer also has tolerance for material purity and optoelectronic properties, [2] as well as allowing for the use of light-weight flexible substrates. Furthermore, of special interest is the strength of the device physics since an ultrathin device offers some key attributes, including better ratio of photocurrent over dark current and improved collection of carriers. The former contributes to a high open-circuit voltage (V_{oc}) and the latter brings to a large Fill Factor (FF).

Although an ultra-thin device benefits from outstanding electrical properties, the thickness of which has posed a challenge for light absorption, limiting the short-circuit current (J_{sc}), and the efficiencies of ultra-thin devices have thus so far lagged behind their crystalline, wafer-based counterparts, mainly because of the insufficient light absorption. The silicon, which is an indirect badgap material, has a low absorption coefficient, in particular, at the near-infrared wavelengths. As a result, In a 10 μm thick silicon, only 30% of the total available current is absorbed [3]. However, the unacceptable photocurrent loss can be addressed by introducing light trapping structure. In the case of ideal lambertian light trapping, the path length can be effectively increased by $4n^2$ [4]. In practical, a texture surface is widely applied to reduce reflection as well as couple light obliquely into the absorbing layer. For thick silicon solar cell, one of the most successful use of the light trapping is the pyramid structure, which has a characteristic feature size of, typically, $3-10$ μm [5]. When the thickness is reduced around sub -10 μm, it is clear that the microscale light trapping structure might not be suitable for the ultrathin device. A great number of approaches have thus been promoted to address the light trapping issue in the ultrathin device, including randomly textured substrates [6–8], photonic nanostructures such as nanowires [9,10], nanocones [11,12] and nanopillars [13,14], and plasmonic structures[15,16]. Although experiments have confirmed significant light absorption enhancement by applying these light trapping strategies, the improvement of the photocurrent, and associated conversion efficiency, is still not commensurate with

* Corresponding author.
E-mail address: gliad@connect.ust.hk (G. Li).

http://dx.doi.org/10.1016/j.solmat.2015.05.042
0927-0248/

the expectation from the result of the optical simulation, mostly due to parasitic optical and electrical losses. Migrating these losses will absolutely lead to high-efficiency devices. For example, $J_{sc} > 30$ mA/cm^2 was achieved in a microcrystalline silicon solar cell using a moth-eye film combined with a honeycomb light trapping structure [17,18], achieving an independently confirmed efficiency of 11.4% [19]; a high efficiency of up to 13.7% was achieved in a sub-10-μm-thick Si solar cell, with an all-back-contact design preventing Auger recombination and with a nanocone structure having less surface area than any other nanostructures for solar cells [20]; Most recently, a 15.7% efficiency 10-μm-thick crystalline silicon solar sell has been also demonstrated by using a 2D nanopyramid surface texture, the measured high short-circuit current of 34.5 mA/cm^2 results from reducing parasitic absorption losses in the back aluminum reflector and nitride anti-reflection coating [21].

Fabrication of the ultra-thin device also involves in making an ultrathin film, if possible, then transferring it to an inexpensive substrate, such as glass or flexible plastic. The challenge of forming the ultrathin film has been investigated in the past [22]. Among the methods there includes a wafering technique called "SLiM-Cut" [23], a lift-off approach based on "Epifree" growth of porous silicon [24], and a seed layer approach based on the formation of a thin polycrystalline silicon layer [25]. Further to the formation, transferring the thin film or ultrathin film single crystal silicon to inexpensive substrates turns out to be even more important, since the freestanding film has its limitation from the point view of the fabrication process and practical application. Recently, the direct wafer bonding technique was successfully applied to achieve a new record efficiency of 44.7% for a GaInP/GaAs//GaInAsP/GaInAs four-junction solar cell [26].

In this paper, we report on the use of an a-Si/c-Si tandem cell to realize a high efficiency solar cell. The use of an ultrathin c-Si cell as the bottom cell is regarded as providing a high degree of freedom with respect to control of the photocurrent when compared with microcrystalline silicon – at least when considering the absorber layer thickness. In addition, the present work presents the use of the anodic bonding process to enable transferring the ultrathin c-Si bottom cell onto the glass substrate. Finally, the conformal deposition on the developed nanoscale inverted pyramid structure, in combination with advanced mixed-phase silicon oxide layers, guarantees a maximum trade-off between optical and electrical performances.

2. Experimental

The layered structure of the ultrathin a-Si/c-Si tandem solar cell is: Glass/Al (200 nm)/n$^+$-Si (0.5 μm)/c-Si absorber (n type,8 μm)/p-a-Si emitter (12 nm)/ITO (Indium tin oxide, 50 nm)/ZnO:Al (25 nm)/n-μc-Si (25 nm)/i-a-Si (300 nm)/p-a-Si (15 nm)/ITO (75 nm), as shown in Fig. 1(a). The schematic illustration of the fabrication process is shown in Fig. 1(b). The process began by the diffusion of an n$^+$ silicon layer in the LPCVD (Low-Pressure Chemical Vapor Deposition), followed by sputtering of 200 nm Al as the back contact, and the handle wafer was bonded to the glass substrate by the anodic bonding process, which was applied at a temperature of 360 °C and bonding voltage of 800 V. An ultrathin 8.5 μm c-Si was achieved with backside etching of the handle wafer that is sequentially done with grinding, polishing, and wet etching in TMAH (Tetramethylammonium hydroxide). The fabrication of the nanoscale inverted pyramid structure on the 8.5 μm ultrathin film includes two main steps: an ultraviolet nanoimprint lithography (UV-NIL) step to replicate the pre-patterned 3D grating from the master in combination with a silicon anisotropic etching step to form the inverted pyramid structure. More details can be found from the previous paper [27]. On the as fabricated inverted nanopyramid structure, a 12 nm p-a-Si hetero-junction emitter was deposited by radio frequency (RF, 13.56 MHz) Plasma Enhanced Chemical Vapor Deposition (PECVD). The sample was then transferred to an sputter (AJA) to deposit the ITO (50 nm) and ZnO:Al (25 nm) as the intermediate layer. Then the n, i and p layers were deposited sequentially in the PECVD. The i-a-Si was fabricated by the RF-PECVD while the n-μc-Si, p-SiO_x and n-SiO_x layers are fabricated by very high frequency (VHF, 60 MHz) PECVD. The deposition temperature for all of these layers was 200 °C. A $SiH_4/H_2/PH_3$(10%)/B_2H_6(1%) precursor gas mixture of 50/10/0/40 is used for the p-a-Si emitter, 50/50/0/0 for the i-a-Si and 5/500/5/0 for the n-μc-Si. The SiO_x layers were produced with a $SiH_4/H_2/PH_3$(10%)/B_2H_6(1%)/CO_2 mixture of 4/500/0/4/2 for the P-SiO_x and 5/500/1/10 for the N-SiO_x. After the deposition of the p-type layer, a 75 nm ITO was sputtered through a shadow mask (the area of the ITO is 0.1 cm²). Before the measurement, silver paste was formed on top of the ITO to make Ohmic contact between the probe and the ITO.

Fig. 2(a) illustrates the schematic of the anodic bonding process. Alkali-rich glass and a silicon wafer coated with 200 nm Al were used as the substrate and handling wafer, respectively. After the cleaning process, the handing wafer and the glass substrate were brought closely together. The glass substrate was contacted with the cathode and the silicon wafer was contacted with the anode. The temperature was elevated to around 360 °C, and then a voltage of 800 V was applied. After the bonding of the handling wafer to the glass, it was thinned to 40–50 μm followed by a grinding and polishing process. The wet etching process in an aqueous TMAH solution (80 °C, 25%) was used to further reduce the thickness to 8.5 μm. After the wet etching, the resulting film surface was relatively smooth and there were no pinholes existing, indicating the bonding process was successful. The defect free bonding process can be tolerant by using a SOI wafer, whereas a SiO_2 layer was used as the etch-stopping layer. In this case, the wet etching process will automatically stop at the SiO_2 surface; therefore, defects, if formed during the bonding process, will not be transferred to the silicon-absorbing layer. After the removal of the SiO_2 layer, a damage free surface was obtained.

Current–voltage characteristics were measured under simulated AM1.5G sunlight at 100 mW/cm^2 irradiance, generated by a 450-W xenon lamp (Oriel, Sol2A) as light source. The light intensity was calibrated using an NREL calibrated Si reference cell. The measurement of the tandem cell is a two-contact measurement in which that the front contact is silver paste (on top of ITO) and the back contact is Al (on the glass side). Pins are contacted with the silver and the Al back contact, respectively. It is also easy to measure the single-junction top or bottom cells by making use of the ITO/ZnO:Al intermediate layer as another terminal. For example: a-Si top cell can be measured with one pin contacted with the silver and the other contacted with the intermediate layer. External quantum efficiency (EQE) measurement was performed with a monochromator, light chopper, and lock-in amplifier (probe beam area 2.5 mm^2, light source: halogen lamp). A calibrated silicon photodiode was used to calibrate the system with uncertainties quoted as 5% for 400 – 1100 nm, A red and a green bias light was used for the top and bottom cell, respectively. Scanning electron microscopy images were obtained using an analytical field emission scanning electron microscopy (JEOL-7100F). Optical measurement was carried out using an integrating sphere to account for reflectance.

The simulation was conducted by using the finite-difference time-domain (FDTD) method. By solving Maxwell's equations, the distribution of the electric and magnetic field intensity could be obtained. With the imaginary part of the permittivity of the materials, it is possible to calculate the absorption directly from

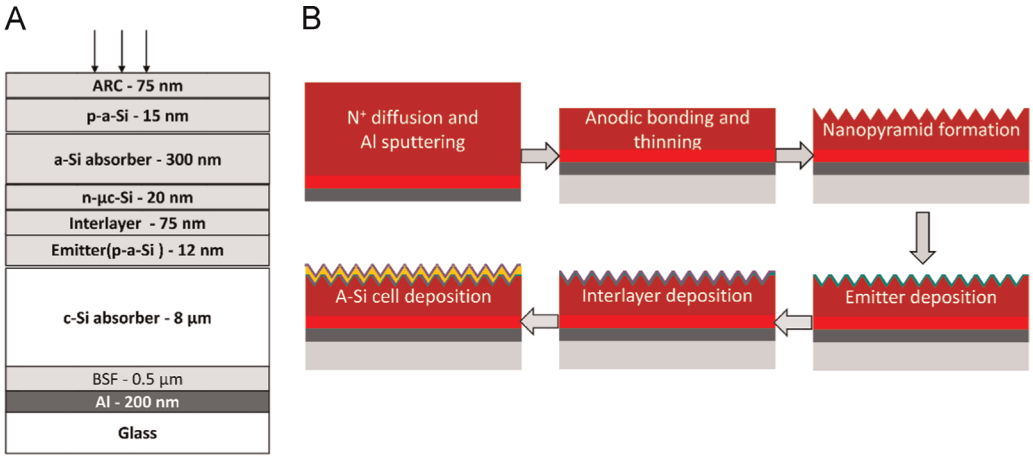

Fig. 1. (a) Ultrathin a-Si/c-Si tandem cell structure; (b) schematic illustration of the fabrication process.

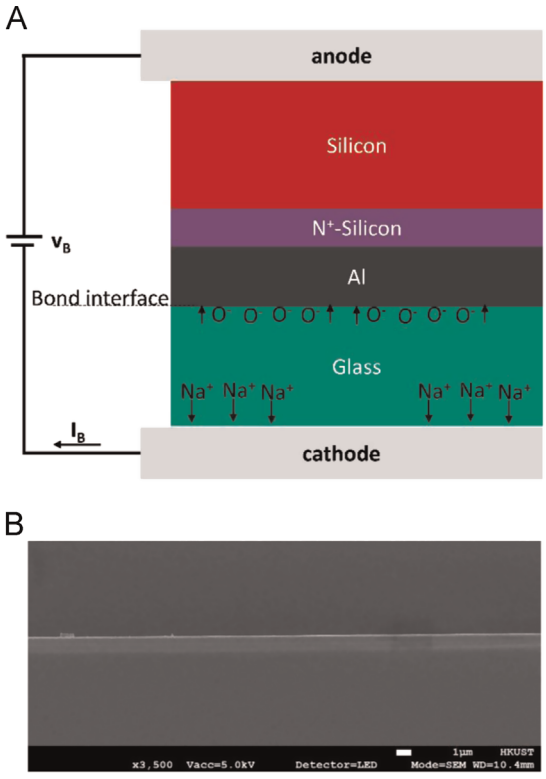

Fig. 2. (a) Schematic of work principle for the anodic bonding process. The cathode is contacted with glass and the anode is contacted with bulk silicon; (b) cross section scanning electron microscope image of the bond interface.

the below formula:

$$P_{abs} = -0.5\omega|E|^2\mathrm{imag}(\varepsilon) \quad (1)$$

3. Results and discussion

3.1. Anodic bonding of ultrathin c-Si bottom cell to glass substrate

Under the applied electrical potential, sodium ions (Na^+) move out of the bond interface to the backside of the glass (cathode), leaving negatively charged oxygen ions (O^-) in the depletion region. It is believed that a thin Al_2O_3 layer will be formed at the bonding interface [28]. Therefore, the wafer and glass are combined ultimately together because of the chemical bonded at the interface. The diffusion of the impurities (positively charged) from the glass into the silicon layer will not occur due to the exist of the applied electrical field, eliminating the possible alkaline contamination from the borosilicate glass. The Al film used here provides a high degree of freedom in the device design. It covers the whole wafer surface, providing electrical contact between the aluminum and buck silicon; it also allows for a high degree of diversity in the fabrication process. For example, it is possible to passivate the backside of the c-Si cell. Meanwhile, the Al layer is provided as the back contact and back reflector in the solar cell structure.

The surface cleanliness and roughness of the glass and silicon wafer are critical to make sure the bonding process works properly. Otherwise, the contamination of large particles may cause bonding defects, and has a large impact on the resulting ultrathin film quality after the wet etching. In our process, we follow a widely established RCA cleaning procedure to remove any surface impurities. The cross section SEM of the bonding interface is shown in Fig. 2(b). Intimate contact is obtained by forming an Al_2O_3 interfacial layer and no defects are observed at the interface.

Hetero-junction ultrathin silicon single junction solar cells are fabricated by forming a p-a-Si emitter and ITO contact on the top surface. Table 1 shows the performance of the ultrathin silicon cells based on the handling wafer (4″ Double-side Polished, 10 Ω cm, n-type float-zone grown silicon wafer) with and without a SiO_2 (100 nm SiO_2) etch-stopping layer (in this case, the SOI wafer is used as the handling wafer). The thickness of the absorbing layers in both cases is 8 μm, with a 0.5 μm n^+ doped layer as the BSF. Efficiencies of 10.3% and 8.9% are obtained for the cell with and without an etch-stopping layer, respectively. The higher efficiency is presumably due to the damaged free surface when the etch-stopping layer is used.

As discussed above, the advantages of ultrathin crystal silicon over microcrystalline silicon as the bottom cell in a tandem cell architecture are its high quality and its freedom of controllable thickness, which gives rise to high V_{oc} and adapted J_{sc} for the bottom cell. In our case, the V_{oc} of the ultrathin cystal silicon solar

Table 1
Performance of 8-μm ultra-thin silicon single junction solar cells based on the handling wafer with and without a SiO_2 etch-stopping layer. An N type wafer is used as the handling wafer without an etch-stopping layer, while the case with a SiO_2 etch-stopping layer, an SOI wafer is used.

Etch-stopping layer	V_{oc} [mV]	J_{sc} [mA/cm^2]	FF [%]	Efficiency [%]
Without	596	30.1	50.0	8.9
With	613	31.2	53.9	10.3

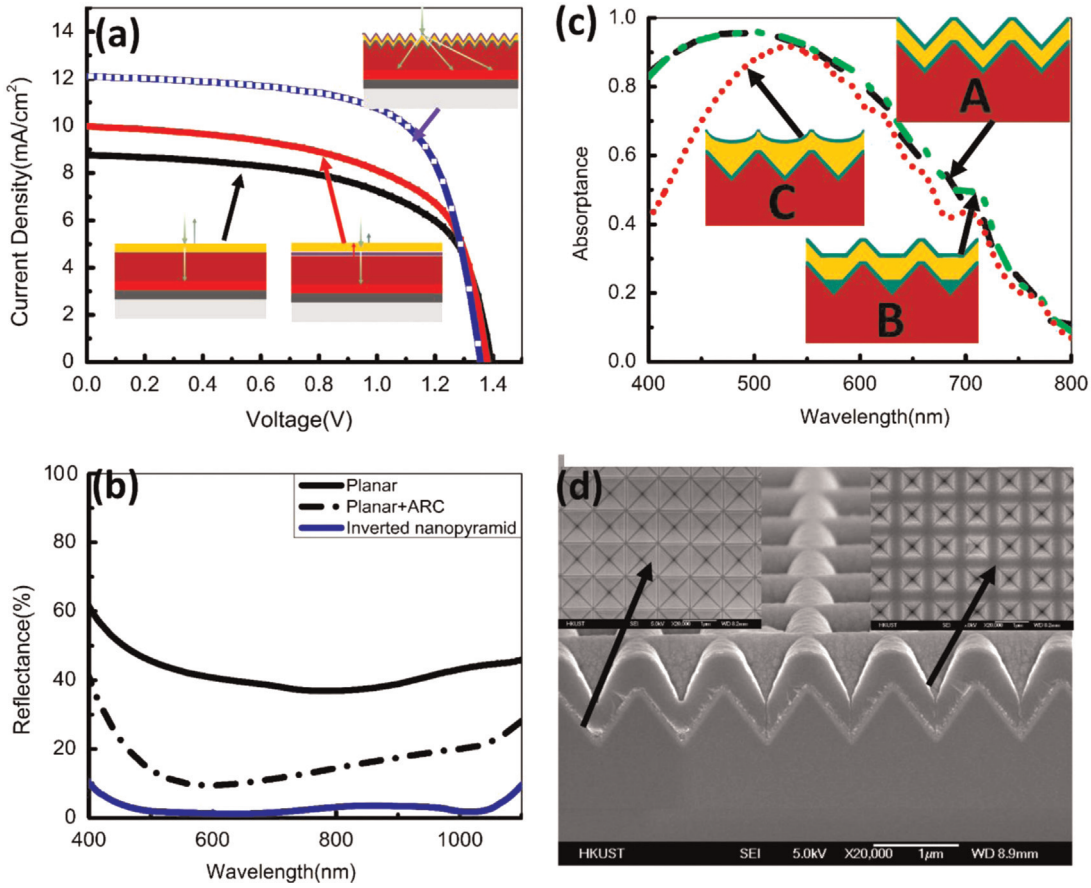

Fig. 3. (a) *J–V* curves of the ultrathin a-Si/c-Si tandem cells with different light trapping structures. The insets illustrate the light behavior in the tandem cells; (b) the reflectance of the tandem cells with a planar surface, a planar surface coated with an anti-reflective coating layer and an inverted nanopyrmaid structure; (c) the light absorption of the tandem cells with different structures from the optical simulation. Structure A has the conformal deposition structure, structure B follows an inverted truncated square nanopyramid, and structure C follows a parabolic cone; (d) the cross section SEM images of an ultrathin a-Si/c-Si tandem cell. The left-hand inset is the top view SEM image of the nanoscale inverted pyramid structure fabricated at the c-Si surface, and right-hand inset is the top view SEM image of the a-Si top cell surface.

cell is 613 mV, much higher than the value normally obtained for μc-Si solar cells [17,18]. In addition, the maximum J_{sc} of μc-Si cells previously reported is around 30.4 mA/cm^2 [19], which is smaller than that of our ultrathin c-Si cell. In practice, V_{oc} of heterojunction cell can be improved above 700 mV [29], and J_{sc} of the ultrathin cell could be further improved if necessary, by simply increasing the thickness or using light trapping schemes.

3.2. Conformal deposition enables efficient light trapping

The tandem cell with 300 nm nip a-Si as the top cell and 8 μm ultrathin c-Si as the bottom cell has a low efficiency of 7.4%, with V_{oc} of 1.39 V, J_{sc} of 8.75 mA/cm^2 and FF of 0.61. The efficiency is mainly limited by the J_{sc} of the top cell, since the 8 μm bottom cell can provide J_{sc} as large as 31.2 mA/cm2. The low J_{sc} of the a-Si top cell is due primarily to the high reflection at the planar top surface, as well as the single pass for the specular incident light in the tandem cell, as demonstrated in the inset of Fig. 3(a). An intermediate layer comprising an AZO/ITO stack is used to partially reflect light back into the top cell to increase the light absorption, and the efficiency is thus improved to 8.3%. The AZO/ITO stack used here is under the consideration of the high conductivity (provided by the ITO) and the resistive surface which adapts to the exposure of the hydrogen-rich plasma environment, because the exposure of the ITO to the hydrogen-rich plasma is found to deteriorate the device performance. Although the intermediate layer can enhance the light absorption of the a-Si to give rise to a high efficiency, the high reflection at the flat top surface and that no oblique light is scattered are still not resolved. Texturing at the surface is necessary to reduce the light reflection. A nanoscale inverted pyramid structure is thus introduced. Unlike previous light trapping structures that were developed at the top or the bottom surfaces of the device, the nanostructure here is first patterned at the surface of the ultrathin c-Si (left-hand inset of Fig. 3(d)), and then the inverted pyramid morphology is transferred to the top cell. As a result, the top surface of the a-Si top cell also shows a textured surface (right-hand inset of Fig. 3(d)).

Fig. 3(b) compares the reflectance of the tandem cells with and without the inverted nanopyramid structure. The planar cell has the highest reflectance due to the large difference in the refractive index of the silicon and air. The reduced light reflection of the device with the inverted nanopyramid structure is obviously observed, with the average reflectance smaller than 8%. Because of the greatly reduced reflection, the cell with the nanoscale inverted pyramid structure shows a large improvement of the J_{sc}. A remarkable gain of 23% and 40% are obtained compared with the cells without and with an intermediate layer. It should be noted that part of the improvement of the J_{sc} is attributed to the enhanced light path length because of the diffraction/scattering effect, the details of which are well discussed in our previous papers [27,30].

In order to get maximization of the light trapping of the a-Si top cell, it is required to have conformal deposition of the a-Si top cell on the nanoscale inverted pyramid structure. Deviation from the conformality will change the surface morphology, resulting in the reduction of the light trapping effect. In order to clarify this

point, light-trapping properties on the deviation from the conformal deposition of the a-Si top cell are investigated by the FDTD simulation. For comparison purposes, three structures are constructed to demonstrate the light absorption of the a-Si top cell, as shown in Fig. 3(c). Structure A has the conformal deposition structure while structures B and C deviate from the conformality. The details of the three structures are as follows: all of the cells have the same layer structures of Glass/Al/c-Si /ITO/ a-Si absorber/ ITO. The thicknesses are the same as that of the real a-Si top cell. For the Structure A cell, the lateral period is 1000 nm. The spacing between the adjacent pyramids is 100 nm, the span along *x* and *y* direction is 900 nm, and the height is 600 nm; structure B and C have the same set, with difference top surfaces described in the inset of Fig. 3(c) that structure B follows an inverted truncated square nanopyramid and structure C follows a parabolic cone. It should be mentioned that the amount of a-Si in structures B and C is larger than that of structure A. Lower absorption is clearly observed for structure C with a parabolic cone structure at the top surface, especially at the short wavelength, which is mainly due to the increased light reflection at the surface because of the variation of the surface morphology. Structure B with an inverted truncated square nanopyramid at the surface shows only a small drop in the absorption, indicating deviation from this way will not cause the a dramatical decrease of the light absorption. In other words, the surface morphology is still kept to ensure low light reflection at the surface.

Fortunately, it is possible to conformally deposit a-Si top cell on the nanopyramid patterned c-Si bottom cell due to the large inclination angle of the inverted pyramid. As shown in Fig. 3(d), the left-hand inset shows the top view of the nanopyramid pattern at the ultrathin c-Si surface while the right-hand inset shows the top view of the pattern after the sequential deposition of the p-a-Si emitter, ITO/AZO intermediate layer and nip a-Si top cell. The top surface of the cell also shows a "pyramid-like" structure, which still retain its period and height, with only the spacing between adjacent pyramids becoming smaller, as compared with the original structure. The a-Si top cell is therefore patterned with an inverted pyramid structure at the bottom and a "pyramid-like" structure at the top. This double-sided light trapping scheme, which we have shown before in [27], can give us the maximization of the light absorption of the a-Si top cell.

3.3. Mixed-phase SiO_x material migrates the electrical loss

The introduction of texturing can greatly enhance the light absorption. However, this is accompanied with parasitic loss, mainly due to the poor quality of the a-Si absorbing layer and the interface. In this section, we show that we can migrate the electrical loss while maximizing the light absorption.

Solar cells with different doped layers are demonstrated in Fig. 4 and characterized as cells S0, S1, S2 and S3. The S0 cell is the reference structure. The differences in S1, S2, and S3 are marked in red. The cell results are summarized in Table 2. There is obvious V_{oc} loss for the S0 cell, which results from the low V_{oc} of the top cell grown on the textured inverted nanopyramid surface. When the p-μc-SiO_x is used as the window layer, as seen from the results of the S1,S2 and S3 cells, the loss of the V_{oc} can be mostly mitigated. The main reason for this improvement, which has been widely reported, is because the shunt current can be efficiently quenched and because of the wide bandgap of the SiO_x layer [31]. In the S2 cell, the p-μc-SiO_x is also used to replace the p-a-Si emitter, trying to achieve the above effect. The performance of this cell does not show any improvement compared with the S1 cell. On the other hand, the V_{oc}, J_{sc} and FF are all lower than those of the S1 cell, leading to a poor efficiency of 12.5%. In the case of the S3 cell, where an n-μc-Si/n-μc-SiO_x bilayer is used to replace the n-μc-Si, the V_{oc} and FF are further improved from 1.45 V and 0.69 to 1.47 V and 0.7, respectively. The electrical improvement indicates the quality of the intrinsic a-Si layer is improved when deposited on the SiO_x layer and the possible shunt path is removed with a bilayer tunneling recombination structure [32]. However, the J_{sc} suffers from parasitic optical loss from the bilayer.

3.4. Solar cell performance

The *IV* curve of the optimized cell with the nanoscale inverted pyramid structure is shown in Fig. 5(a), with an obtained V_{oc} of 1.47 V, J_{sc} of 13.2 mA/cm^2 FF of 0.7 and power conversion efficiency of 13.6%. It should be noted that the performance is initial and usually exhibits degradation upon light soaking. The high V_{oc} is almost the sum of the top cell (0.87 V) and bottom cell (0.605 V), indicating there is almost no voltage loss in the tunneling recombination junction. The external quantum efficiency (EQE) is shown in the inset of Fig. 5(a). The integrated EQE is in good agreement with that measured from *J–V* measurement, with the top cell limited (top cell current smaller than bottom cell current). As compared with the planar cell, the large improvement comes from the J_{sc}, indicating the superior light trapping capability of the

Table 2
Performance of tandem cells with difference doping layers. The listed in the table comes from the best cell.

Cell structure	V_{oc} [mV]	J_{sc} [mA/cm^2]	FF [%]	Efficiency [%]
S0	1.37	13.0	0.66	11.8
S1	1.45	13.4	0.69	13.4
S2	1.43	13.2	0.66	12.5
S3	1.47	13.0	0.70	13.4

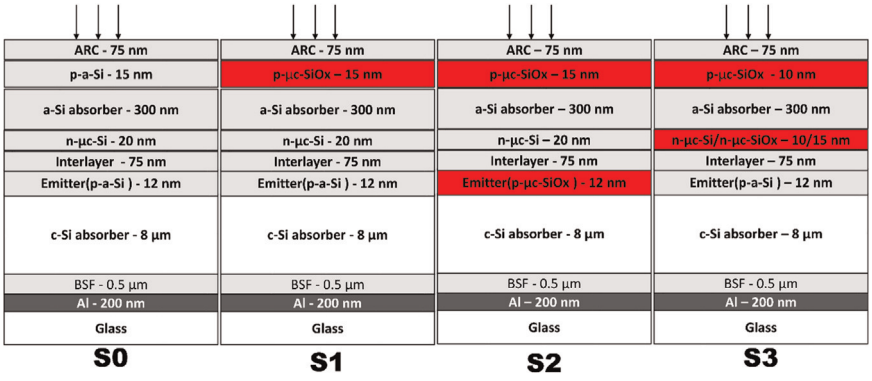

Fig. 4. a-Si/c-SI tandem cell structure with different doping layers. S0 is the reference cell. The difference in S1, S2 and S3 cells are marked with red. (For interpretation of the references to color in this figure legend, the reader is referred to the web version of this article.)

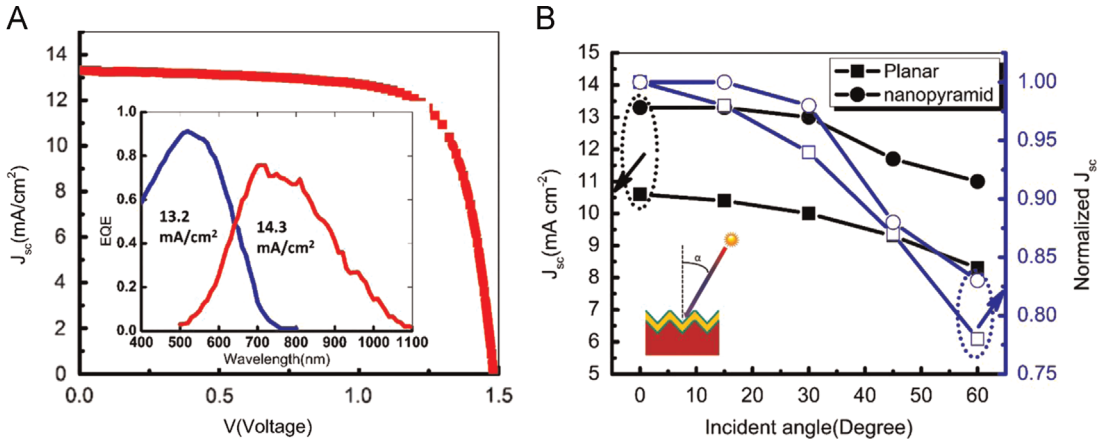

Fig. 5. (a) *J–V* curve of the optimized cell with the inverted nanopyramid light trapping structure, inset is the corresponding external quantum efficiency; (b) short-circuit current measured at simulated AM1.5g spectral with different incident angles.

inverted nanopyramid structure, which results from the antireflection effect and the diffraction effect. It should be noted that, as reported before, the inverted nanopyramid structure at the a-Si and c-Si interface also plays an important role as the diffractive intermediate layer to increase not only the current of the top cell, but also of the bottom cell [30].

The *J–V* measurement is carried out with normal incident light, but for practical applications, the incident sunlight changes angle over time and cell efficiency depends on the incident angle of the sunlight. It is thus important to investigate the angle dependent power output. Because the incident angle is mainly responsible for the light absorption, we compare the J_{sc} of the planar and nanopyramid cells as shown in Fig. 5(b). Intriguingly, it can be clearly seen that the J_{sc} of the nanopyramid device remains unchanged at 15% for incident angles. However, it decreases to 98% for the planar cell. Both cells continue this decrease when continuing to increase the incident angle from 15° to 60°, but it seems that the nanopyramid cell performes better than the planar cell. Further studies are needed to clarify this behavior and are beyond of our present studies.

4. Conclusions

In conclusion, we have proposed here an ultra-thin, high performance a-Si/c-Si tandem cell fabricated on a glass substrate. We demonstrate that the ultrathin film can be successfully transferred to the inexpensive glass substrate using the anodic bonding process. The bonding process is a useful technique to develop the ultrathin film device. In addition, we apply a nanoscale inverted pyramid structure to achieve the light absorption of the tandem cell. The conformal deposition of the sequential layers on such a nanostructure enables maximizing the light trapping capability. On the other hand, deviation from the conformal deposition will induce a decrease of the light trapping. By further removing the parasitic loss, an impressive high efficiency of up to 13.6% was achieved for the ultra-thin tandem cell. Finally, we compare the output performances of cell with and without nanopyramid light trapping structure, considering the practical application by measuring the *J–V* curves at different incident angles. We show that the tandem cell with the nanopyramid structure shows a better performance with a large incident angle when compared with that of the planar cell. It should be noted that our hetero-junction c-Si cell is still far from fully optimized. The efficiency of our tandem cell could be further improved to 16% by continuing to do the passivation process of the ultrathin c-Si heterojuntion solar cell. However, our work suggests a viable path toward high-efficiency ultrathin solar cells.

Acknowledgment

This work was supported by the Innovation and Technology Commission of Hong Kong Government under Grant no. GHP/058/09SZ.

References

[1] D.M. Powell, M.T. Winkler, A. Goodrich, T. Buonassisi, Modeling the cost and minimum sustainable price of crystalline silicon photovoltaic manufacturing in the United States, IEEE J. Photovolt. 3 (2013) 662–668.
[2] J.Y. Kwon, D.H. Lee, M. Chitambar, S. Maldonado, A. Tuteja, A. Boukai, High efficiency thin upgraded metallurgical-grade silicon solar cells on flexible substrates, Nano Lett. 12 (2012) 5143–5147.
[3] ⟨http://pveducation.org/pvcdrom/design/material-thickness⟩, 2015.
[4] T. Tiedje, E. Yablonovich, G.D. Cody, B.G. Brooks, Limiting efficiency of silicon solar cells, IEEE Trans. Electron Devices 31 (5) (1984) 711–716.
[5] P. Campbell, M.A. Green, Light trapping properties of pyramidally textured surfaces, J. Appl. Phys. 62 (1987) 243–249.
[6] J. Müller, B. Rech, J. Springer, M. Vanecek, TCO and light trapping in silicon thin film solar cells, Sol. Energy. 77 (2004) 917–930.
[7] H. Sai, H. Jia, M. Kondo, Impact of front and rear texture of thin-film microcrystalline silicon solar cells on their light trapping properties, J. Appl. Phys. 108 (2010) 044505.
[8] C. Battaglia, C.-M. Hsu, K. Söderström, J. Escarré, F.-J. Haug, M. Charrière, et al., Light trapping in solar cells: can periodic beat random? ACS Nano 6 (2012) 2790–2797.
[9] E. Garnett, P. Yang, Light trapping in silicon nanowire solar cells, Nano Lett. 10 (2010) 1082–1087.
[10] L. Tsakalakos, J. Balch, J. Fronheiser, B.A. Korevaar, O. Sulima, J. Rand, Silicon nanowire solar cells, Appl. Phys. Lett. 91 (2007) 233117.
[11] C.-M. Hsu, C. Battaglia, C. Pahud, Z. Ruan, F.-J. Haug, S. Fan, et al., High-efficiency amorphous silicon solar cell on a periodic nanocone back reflector, Adv. Energy Mater. 2 (2012) 628–633.
[12] J. Zhu, Z. Yu, G.F. Burkhard, C.-M. Hsu, S.T. Connor, Y. Xu, et al., Optical absorption enhancement in amorphous silicon nanowire and nanocone arrays, Nano Lett. 9 (2009) 279–282.
[13] Z. Fan, D.J. Ruebusch, A.A. Rathore, R. Kapadia, O. Ergen, P.W. Leu, et al., Challenges and prospects of nanopillar-based solar cells, Nano Res. 2 (2009) 829–843.
[14] G. Mariani, A.C. Scofield, C.-H. Hung, D.L. Huffaker, GaAs nanopillar-array solar cells employing in situ surface passivation, Nat. Commun. 4 (2013) 1497.
[15] P. Spinelli, V.E. Ferry, J. van de Groep, M. van Lare, M.A. Verschuuren, R.E. I. Schropp, et al., Plasmonic light trapping in thin-film Si solar cells, J. Opt. 14 (2012) 024002.
[16] V.E. Ferry, M.A. Verschuuren, H.B. Li, E. Verhagen, R.J. Walters, R.E. Schropp, et al., Light trapping in ultrathin plasmonic solar cells, Opt. Express. 18 (2010) A237–A245.
[17] H. Sai, T. Matsui, K. Matsubara, M. Kondo, I. Yoshida, 11.0%-efficient thin-film microcrystalline silicon solar cells with honeycomb textured substrates, IEEE J. Photovolt. 4 (2014) 1349–1353.
[18] H. Sai, T. Matsui, K. Saito, M. Kondo, I. Yoshida, Photocurrent enhancement in thin-film silicon solar cells by combination of anti-reflective sub-wavelength

structures and light-trapping textures: photocurrent enhancement in thin-film silicon solar cells, Prog. Photovolt. Res. Appl. (2015), http://dx.doi.org/10.1002/pip.2594, n/a–n/a.
[19] M.A. Green, K. Emery, Y. Hishikawa, W. Warta, E.D. Dunlop, Solar cell efficiency tables (version 45): solar cell efficiency tables, Prog. Photovolt. Res. Appl. 23 (2015) 1–9.
[20] S. Jeong, M.D. McGehee, Y. Cui, All-back-contact ultra-thin silicon nanocone solar cells with 13.7% power conversion efficiency, Nat. Commun. 4 (2013).
[21] M.S. Branham, W.-C. Hsu, S. Yerci, J. Loomis, S.V. Boriskina, B.R. Hoard, et al., 15.7% efficient 10-μm-thick crystalline silicon solar cells using periodic nanostructures, Adv. Mater. 27 (2015) 2182–2188.
[22] I. Gordon, F. Dross, V. Depauw, A. Masolin, Y. Qiu, J. Vaes, et al., Three novel ways of making thin-film crystalline-silicon layers on glass for solar cell applications, Sol. Energy Mater. Sol. Cells. 95 (2011) S2–S7.
[23] F. Dross, A. Milhe, J. Robbelein, I. Gordon, P.-O. Bouchard, G. Beaucarne, et al., Stress-induced lift-off method for kerf-loss-free wafering of ultra-thin (50 μm) crystalline Si wafers, in: Proceedings of the 33rd IEEE Photovoltic Specialist Conference 2008 PVSC08, IEEE, 2008, pp. 1–5. ⟨http://ieeexplore.ieee.org/xpls/abs_all.jsp?arnumber=4922741⟩ (accessed 03.04.15).
[24] I. Mizushima, T. Sato, S. Taniguchi, Y. Tsunashima, Empty-space-in-silicon technique for fabricating a silicon-on-nothing structure, Appl. Phys. Lett. 77 (2000) 3290.
[25] I. Gordon, L. Carnel, D. Van Gestel, G. Beaucarne, J. Poortmans, 8% Efficient thin-film polycrystalline-silicon solar cells based on aluminum- induced crystallization and thermal CVD, Prog. Photovolt. Res. Appl. 15 (2007) 575–586.
[26] F. Dimroth, M. Grave, P. Beutel, U. Fiedeler, C. Karcher, T.N.D. Tibbits, et al., Wafer bonded four-junction GaInP/GaAs//GaInAsP/GaInAs concentrator solar cells with 44.7% efficiency: wafer bonded four-junction concentrator solar cells with 44.7% efficiency, Prog. Photovolt. Res. Appl. 22 (2014) 277–282.
[27] G. Li, H. Li, J.Y.L. Ho, M. Wong, H.S. Kwok, Nanopyramid structure for ultrathin c-Si tandem solar cells, Nano Lett. 14 (2014) 2563–2568.
[28] K. Schjølberg-Henriksen, E. Poppe, S. Moe, P. Storås, M.M.V. Taklo, D.T. Wang, et al., Anodic bonding of glass to aluminium, Microsyst. Technol. 12 (2006) 441–449.
[29] K. Masuko, M. Shigematsu, T. Hashiguchi, D. Fujishima, M. Kai, N. Yoshimura, et al., Achievement of more than 25% conversion efficiency with crystalline silicon heterojunction solar cells, IEEE J. Photovolt. 4 (2014) 1433–1435.
[30] G. Li, J.Y.L. Ho, H. Li, H.-S. Kwok, Diffractive intermediate layer enables broadband light trapping for high efficiency ultrathin c-Si tandem cells, Appl. Phys. Lett. 104 (2014) 231113.
[31] M. Despeisse, G. Bugnon, A. Feltrin, M. Stueckelberger, P. Cuony, F. Meillaud, et al., Resistive interlayer for improved performance of thin film silicon solar cells on highly textured substrate, Appl. Phys. Lett. 96 (2010) 073507.
[32] L. Gui-Jun, H. Guo-Fu, H. Xiao-Yan, Y. Yu-Jie, W. Chang-Chun, S. Jian, et al., The study of a new n/p tunnel recombination junction and its application in a-Si: H/μc-Si: H tandem solar cells, Chin. Phys. B 18 (2009) 1674.